Smartphone Battery Life Prediction and Sensitivity Analysis Integrating Electrothermal Coupling Dynamics and Stochastic Processes

Yukang Lu[1,*]
[1]College of Mechanical and Electrical Engineering, Hohai University, Changzhou 213200, China
Corresponding author: Yukang Lu (email: yukang-lu@hhu.edu.cn).

ABSTRACT Addressing the highly nonlinear and stochastic nature of smartphone battery depletion, this study establishes a comprehensive dynamic modeling and prediction framework. First, by incorporating the modified Nernst equation and Kirchhoff's voltage law, a fundamental model of nonlinear discharge is established. Building upon this, thermodynamic equilibrium equations are coupled to quantify the feedback mechanisms among Joule heating, internal resistance, and temperature. To replicate real-world complex usage environments, the study innovatively introduced the "Tail Effect" to characterize the high-power-consumption idle state of network modules following data transmission, and utilized Gaussian white noise and Brownian motion to model user interaction behavior as a stochastic process. Experimental results demonstrate that the model achieves extremely high prediction accuracy in typical scenarios such as gaming and social media, with a coefficient of variation consistently below 6% in low-load scenarios. Furthermore, the study thoroughly examined the impact of environmental factors, finding that extreme temperatures significantly accelerate battery capacity degradation; the cycle life at 65 °C is only about one-fifth of that at 35 °C. Through multidimensional sensitivity analysis, the study further identified processor load as the primary energy-consuming factor during high-intensity tasks, while communication traces are a significant source of energy loss in sporadic interaction scenarios. This study provides scientific and quantitative support for energy management and battery life prediction in mobile devices.

INDEX TERMS Electrothermal coupling, stochastic dynamics, sensitivity analysis.

I. INTRODUCTION

AGAINST the backdrop of modern smartphones serving as digital hubs, the nonlinear depletion of battery power and the uncertainty of predictions have long been critical challenges in user experience. Existing battery life predictions often rely on simple linear extrapolation, making it difficult to capture the complex coupling mechanisms among screen brightness, processor load, and hidden background network activity. Although previous studies have made progress in electrochemical modeling, most have overlooked the real-time feedback of temperature on internal resistance and the stochastic fluctuations caused by user behavior. The innovation of this study lies in constructing an iterative optimization framework that bridges "ideal dynamics" and "stochastic loads," deeply integrating the electrothermal balance model at the physical layer with the communication trace effects at the system layer, and introducing stochastic differential equations to quantify prediction uncertainty [1], [2]. The research approach in this section begins with the construction of a basic model, followed by parameter calibration using nonlinear least squares methods, then proceeds to multi-scenario simulation and prediction, and finally evaluates the model's robustness and environmental adaptability through sensitivity testing, with the aim of establishing a highly versatile energy evaluation system [3].

II. MODEL CONSTRUCTION

In this section, we employ an Iterative Modeling Strategy to progressively approximate the complex discharge dynamics of smartphone batteries in real-world scenarios. Adhering to a "simple-to-complex" philosophy, we first establish a basic model to determine the core non-linear mapping among "Charge-Voltage-Power." Subsequently, we introduce thermodynamic laws to construct an electro-thermal coupled system. Finally, we develop a fine-grained component power consumption model incorporating the "Tail Effect" mechanism and stochastic uncertainty to simulate realistic usage environments [4]–[6].

A. BASIC MODEL

We commence by constructing a benchmark model. At this stage, we assume the battery operates in a constant room temperature environment ($T_{\text{amb}} = 298$ K), temporarily disregarding the influence of dynamic temperature fluctuations on internal chemical reaction rates.

The state evolution of a battery system is strictly governed by its Open Circuit Voltage (OCV), denoted as electromotive force E. While the classical Nernst Equation offers a theoretical foundation, its logarithmic term exhibits numerical singularities at SOC boundaries [7]. To enhance numerical stability, we adopt an engineering approach based on Taylor series expansion, utilizing a high-order polynomial approximation. The modified electromotive force $E(\text{SOC})$ is expressed as:

$$E(\text{SOC}) = E_0 - R_T \sum_{k=0}^{5} a_k \cdot \text{SOC}(t)^k \tag{1}$$

where E_0 is the standard reference potential, and the coefficients a_k are determined via least squares fitting of empirical OCV curves [8], [9].

Modern smartphones typically exhibit Constant Power Load (CPL) characteristics [2]. As the battery terminal voltage drops, the loop current $I(t)$ must automatically increase to maintain a constant power output P_{load}. Based on Kirchhoff's Voltage Law (KVL):

$$P_{\text{load}} = V_{\text{term}}(t)I(t) = (E(\text{SOC}) - I(t)r_0)\, I(t) \tag{2}$$

Solving this quadratic equation for the instantaneous current $I(t)$ (taking the physically meaningful smaller root):

$$I(t) = \frac{E(\text{SOC}) - \sqrt{E(\text{SOC})^2 - 4r_0 P_{\text{load}}}}{2r_0} \tag{3}$$

Equation (2) reveals a positive feedback mechanism: SOC $\downarrow \Rightarrow V_{\text{term}} \downarrow \Rightarrow I(t) \uparrow$, which explains the accelerated power depletion observed at low battery levels.

Based on the Coulomb Counting principle [10]–[12], we introduce two critical correction factors to refine the state-space equation: the Aging Factor (δ) and the Temperature Efficiency Coefficient (ε). Let C_0 be the nominal capacity. The differential equation for SOC evolution is:

$$\begin{aligned}\frac{d\text{SOC}(t)}{dt} &= -\frac{1}{C_{\text{actual}}} I(t) \\ &= -\frac{1}{C_0 \cdot \delta \cdot \varepsilon} \frac{E(\text{SOC}) - \sqrt{E(\text{SOC})^2 - 4r_0 P_{\text{load}}}}{2r_0}\end{aligned} \tag{4}$$

The Temperature Efficiency Coefficient ε is modeled as a piecewise function to reflect reduced chemical activity at low temperatures:

$$\varepsilon = \begin{cases} 1, & T > T_0, \\ 1 + \mu \arctan\left(\dfrac{T - T_0}{\Delta}\right), & T \le T_0, \end{cases} \tag{5}$$

where T_0 is the threshold temperature, and μ, Δ are fitting parameters.

B. THE IMPROVED MODEL: ELECTRO-THERMAL COUPLED DYNAMICS

The basic model relies on an "Isothermal Assumption". Since the internal resistance r_0 is highly sensitive to temperature, we expand the system into an Electro-Thermal Coupled System [13]–[15].

1) THERMODYNAMIC BALANCE EQUATION

Treating the battery as a homogeneous system, the evolution of temperature $T(t)$ depends on the balance between heat generation (Q_{gen}) and heat dissipation (Q_{diss}):

$$mC_p \frac{dT(t)}{dt} = Q_{\text{gen}}(t) - Q_{\text{diss}}(t) \tag{6}$$

Heat Generation (Q_{gen}): Includes Joule heating and thermal conduction from the motherboard (coefficient γ):

$$Q_{\text{gen}}(t) = I(t)^2 r_0(T) + \gamma P_{\text{load}} \tag{7}$$

Heat Dissipation (Q_{diss}): Based on Newton's Law of Cooling:

$$Q_{\text{diss}}(t) = hA_{\text{surf}}\,(T(t) - T_{\text{amb}}) \tag{8}$$

2) ARRHENIUS CHARACTERISTICS

We employ the Arrhenius Equation to characterize the non-linear temperature dependence of internal resistance [16]:

$$r_0(T) = r_{\text{ref}} \exp\left[\frac{E_a}{R_g}\left(\frac{1}{T(t)} - \frac{1}{T_{\text{ref}}}\right)\right] \tag{9}$$

3) FINAL COUPLED SYSTEM OF ODES

Combining equations (4), (6), and (9), we derive the system equations for the state vector $x = [\text{SOC}, T]^T$:

$$\begin{aligned}\frac{d\text{SOC}}{dt} &= -\frac{E(\text{SOC}) - \sqrt{E(\text{SOC})^2 - 4r_0(T)P_{\text{load}}}}{2r_0(T)C_0 \cdot \delta \cdot \varepsilon}, \\ mC_p \frac{dT}{dt} &= I(t)^2 r_0(T) + \gamma P_{\text{load}} - hA_{\text{surf}}\,(T - T_{\text{amb}})\,.\end{aligned} \tag{10}$$

C. TOTAL POWER CONSUMPTION MODEL WITH WAKE EFFECT

In reality, P_{load} is a dynamic superposition of multiple factors. We model the total load $P_{\text{load}}(t)$ as:

$$\begin{aligned}P_{\text{load}}(t) = P_{\text{screen}}(t) + P_{\text{cpu}}(t) + P_{\text{gpu}}(t) \\ + P_{\text{network}}(t) + P_{\text{background}}(t)\end{aligned} \tag{11}$$

We employ regression analysis to characterize each component:

Screen: Non-linear coupling of brightness (B) and color (RGB):

$$P_{\text{screen}} = k_{s1} \cdot B + k_{s2} \cdot \text{RGB} + k_{s3} \cdot (B \cdot \text{RGB}) \tag{12}$$

Processor: Polynomial fitting of frequency f:

$$\begin{aligned}P_{\text{cpu}}(f) &= \alpha_1 f_{\text{cpu}} + \alpha_2 f_{\text{cpu}}^2 + \alpha_3 f_{\text{cpu}}^3 + C_{\text{cpu}}, \\ P_{\text{gpu}}(f) &= \beta_1 f_{\text{gpu}} + \beta_2 f_{\text{gpu}}^2 + C_{\text{gpu}}.\end{aligned} \tag{13}$$

Network and "Tail Effect":

$$P_{\text{network}} = \alpha \cdot T_{\text{MB}} - \beta \cdot \log_{10}(T_{\text{Bytes}}) + \gamma \tag{14}$$

The specific models are:

$$\begin{aligned} P_{\text{wifi}} &= \alpha_0 \cdot T_{\text{MB}} + \beta_0 \cdot \log_{10}(T_{\text{Bytes}}) + \gamma_0, \\ P_{\text{cellular}} &= \alpha_1 \cdot T_{\text{MB}} + \beta_1 \cdot \log_{10}(T_{\text{Bytes}}) + \gamma_1. \end{aligned} \tag{15}$$

1) UNCERTAINTY QUANTIFICATION

To simulate the stochastic nature of the real world, we introduce random processes:

Gaussian White Noise: For high-frequency fluctuations (clicks/switching), noise is superimposed on foreground components:

$$P^*_{\text{component}}(t) = P_{\text{component}}(t) + \xi(t), \quad \xi(t) \sim \mathcal{N}(0, \sigma^2_{\text{user}}) \tag{16}$$

Brownian Motion: Addressing the unpredictability of background tasks, we model this using a Wiener Process:

$$P_{\text{background}}(t) = P_{\text{base}} + \sigma_b W(t) \tag{17}$$

where $W(t)$ satisfies the independent increment property: $W(t + \Delta t) - W(t) \sim N(0, \Delta t)$.

III. PROBLEM SOLVING

A. PARAMETER ESTIMATION AND MODEL FITTING

To transition the theoretical model established in Chapter 3 into an executable predictive tool, we utilized a real-world smartphone power consumption dataset sourced from Kaggle [17] and Stanford University. We applied non-linear least squares regression to rigorously calibrate the power equations for each component, successfully deriving robust empirical formulas. These formulas serve as the basis for the subsequent iterative solution of the State of Charge (SOC). The resulting empirical power equations for each module are as follows:

$$P_{\text{screen}} = -0.2964B + 0.2515\text{RGB} + 0.010488(B \cdot \text{RGB}) \tag{18}$$

$$P_{\text{cpu}} = -491.32 f_{\text{cpu}} + 1341.56 f^2_{\text{cpu}} - 194.38 f^3_{\text{cpu}} - 48.79 \tag{19}$$

$$P_{\text{gpu}} = 109.88 f_{\text{gpu}} + 307.97 f^2_{\text{gpu}} + 6.79 \tag{20}$$

$$P_{\text{wifi}} = 6.44 T_{\text{MB}} - 3.36 \log_{10}(T_{\text{Bytes}}) + 210.05 \text{ (mW)} \tag{21}$$

$$P_{\text{cellular}} = 8.54 T_{\text{MB}} - 4.51 \log_{10}(T_{\text{Bytes}}) + 449.22 \text{ (mW)} \tag{22}$$

To verify the reliability of the aforementioned parameter estimation, we introduced the Coefficient of Determination (R^2) and the Normalized Root Mean Square Error (NRMSE) as evaluation metrics. The calculation formulas are:

$$R^2 = 1 - \frac{\sum_{i=1}^{n}(y_i - \hat{y}_i)^2}{\sum_{i=1}^{n}(y_i - \bar{y})^2} \tag{23}$$

$$\text{NRMSE} = \frac{\sqrt{\frac{1}{n}\sum_{i=1}^{n}(y_i - \hat{y}_i)^2}}{y_{\max} - y_{\min}} \times 100\% \tag{24}$$

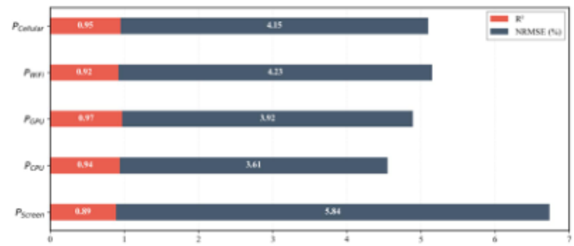

FIGURE 1. R2 and NRMSE of component power fitting

where y represents the observed value, $\hat{y}$ is the predicted value, and $\bar{y}$ is the mean of observations. The fitting performance for each component is illustrated in Figure 1.

The parameter fitting demonstrates exceptionally high precision and robustness. The coefficient of determination (R^2) for all modules exceeds 0.89, and the normalized error for each module is strictly controlled within 6%, with the maximum being only 5.84%. These high-precision equations provide reliable data support for subsequent temporal predictions [18], [19].

B. EXPERIMENTAL SETUP AND SCENARIO INITIALIZATION

Prior to initiating numerical simulations, we first parameterized the model's input space. To encompass diverse battery discharge patterns, we defined four representative usage scenarios: Immersive Gaming, Video Streaming, Long Reading, and Social Snacking. We defined the feature parameter for each scenario. The specific parameter settings are detailed in Table 1.

Parameter initialization for typical usage scenarios is shown in Table 1.

Based on these parameters, we calculated the baseline hardware power for each scenario at $t = 0$. To realistically replicate the physical environment, we introduced a hybrid stochastic perturbation mechanism on top of the baseline:

We utilized Gaussian white noise (standard deviation $=$ 0.1) to simulate power oscillations caused by instantaneous user interactions such as clicking and sliding.

We implemented Geometric Brownian Motion (initial value 500mW, drift 0.5, volatility 0.1) to characterize the cumulative power drift generated by background applications over time.

Ultimately, this total load model, fusing physical laws with stochastic processes, combined with standard battery parameters (3582 mAh) and a 4th-order Runge-Kutta solver, provides a high-fidelity simulation environment for capturing battery depletion behavior under various operating conditions [20].

C. MULTI-SCENARIO DETERMINISTIC TIME-TO-EMPTY PREDICTION AND ANALYSIS

We first conducted numerical simulations for the Time-to-Empty (TTE) across the four typical scenarios under deterministic conditions (ignoring Gaussian and Brownian

TABLE 1. PARAMETER INITIALIZATION FOR TYPICAL USAGE SCENARIOS

Parameter	Symbol	Unit	Gaming	Video	Reading	Social
Screen Brightness	B	%	90	20	40	60
Pixel Grayscale	RGB	0–255	240	200	200	200
CPU Frequency	f_{cpu}	GHz	2.4	0.4	0.8	1.6
GPU Frequency	f_{gpu}	GHz	0.8	0.5	0.4	0.5
Data Rate	D_{MB}	MB/s	2.0	0.3	0.0	0.1
Network Mode	–	–	WiFi	WiFi	WiFi	WiFi

perturbations). We tested five different initial battery levels ($\mathrm{SOC}_0 \in \{20\%, 40\%, 60\%, 80\%, 100\%\}$). The simulation results are shown in Figure 2.

The simulation results in Figure 2 display the SOC decline trajectories under different initial conditions. A comparison reveals that the "Immersive Gaming" scenario exhibits an extremely rapid power depletion rate, with a full-charge endurance of only approximately 3.66 hours. In contrast, the low-load scenario "Reading" show significantly flatter curves, achieving endurance times of over 10 hours, respectively, demonstrating excellent energy efficiency in low-power modes.

Notably, the curves exhibit non-linear characteristics at the tail end: in the low battery interval ($\mathrm{SOC} < 15\%$), the discharge curve shows an "accelerated drop" consistent with physical laws. This is due to the increase in internal resistance and accelerated voltage drop caused by internal chemical reactions, verifying that the differential equation model correctly reflects the electrochemical non-linearities of the battery.

D. MODEL VALIDATION

In reality, users rarely engage in a single activity continuously for several hours. To validate the model's predictive capability in a complex, real-world environment, we defined a mixed weighted process, consisting of 10% Gaming, 20% Music, 20% Reading, and 50% Social.

$$P_{\mathrm{comp}} = 0.1P_{\mathrm{game}} + 0.2P_{\mathrm{music}} + 0.2P_{\mathrm{read}} + 0.5P_{\mathrm{social}} \quad (25)$$

To assess accuracy, we compared the model's predicted full-charge endurance T_{pred} for this synthetic scenario with standardized test data T_{real} for the same device model from reputable Tech Reviewers. The comparison is shown in Figure 3.

E. UNCERTAINTY QUANTIFICATION AND MODEL PERFORMANCE EVALUATION

To quantify the credibility of our predictions, we employed Monte Carlo simulations. The quantification results are illustrated in Figure 4.

Figure 4 presents the TTE distribution including 95% Confidence Intervals (95% CI). The results indicate that the Time-to-Empty is a probability distribution rather than a fixed value. Significant differences in prediction uncertainty exist across scenarios. To systematically evaluate the model's performance under different conditions, we introduced the Coefficient of Variation (CV) as an evaluation metric, calculated as:

$$\mathrm{CV} = \frac{\text{Standard Deviation}}{\text{Mean}} \times 100\% \quad (26)$$

As shown in Figure 5, the heatmap intuitively reveals the evolution of prediction uncertainty with load intensity and remaining power.

Based on this assessment, the core strength of the model lies in handling daily scenarios with medium-to-low loads and medium-to-high battery levels, where the CV value stabilizes within 7%, indicating high prediction accuracy and robustness. Conversely, the model's limitations are concentrated in high-load conditions, where the fluctuation range of prediction results is larger ($\mathrm{CV} > 10\%$).

F. POWER DRAIN FACTOR ANALYSIS

To deeply investigate the specific physical mechanisms leading to rapid battery depletion under different operating conditions, we performed a component decomposition analysis of the average load power for the four typical scenarios.

As shown in Figure 6, the energy consumption decomposition intuitively reveals the direct causes of rapid battery drain. In the "Immersive Gaming" scenario, the combined energy consumption of the computing units—CPU (62.7%) and GPU (13.4%)—exceeds 76%. Meanwhile, the Screen accounts for 18%–36% in Reading and Streaming scenarios. Surprisingly, background energy consumption is controlled within 5% across all scenarios. Network Impact Analysis: Wi-Fi vs Cellular in the Immersive Gaming scenario is shown in Figure 7.

IV. IMPACT OF ENVIRONMENTAL FACTORS ON PREDICTION RESULTS

As can be seen from the figure above, endurance is longest at 10°C (5.85 hours), followed by 0°C (4.96 hours) and 20°C (5.45 hours). Excessively high or low temperatures shorten battery life. Screen Brightness is shown in Figure 8. Seasonal impact on battery life (video streaming scenario) is shown in figure 9.

A. BATTERY AGING MECHANISMS AND STRATEGY

Battery aging is a complex electrochemical degradation process characterized by two primary manifestations: capacity fade and internal resistance growth. To systematically quantify battery health deterioration over its operational

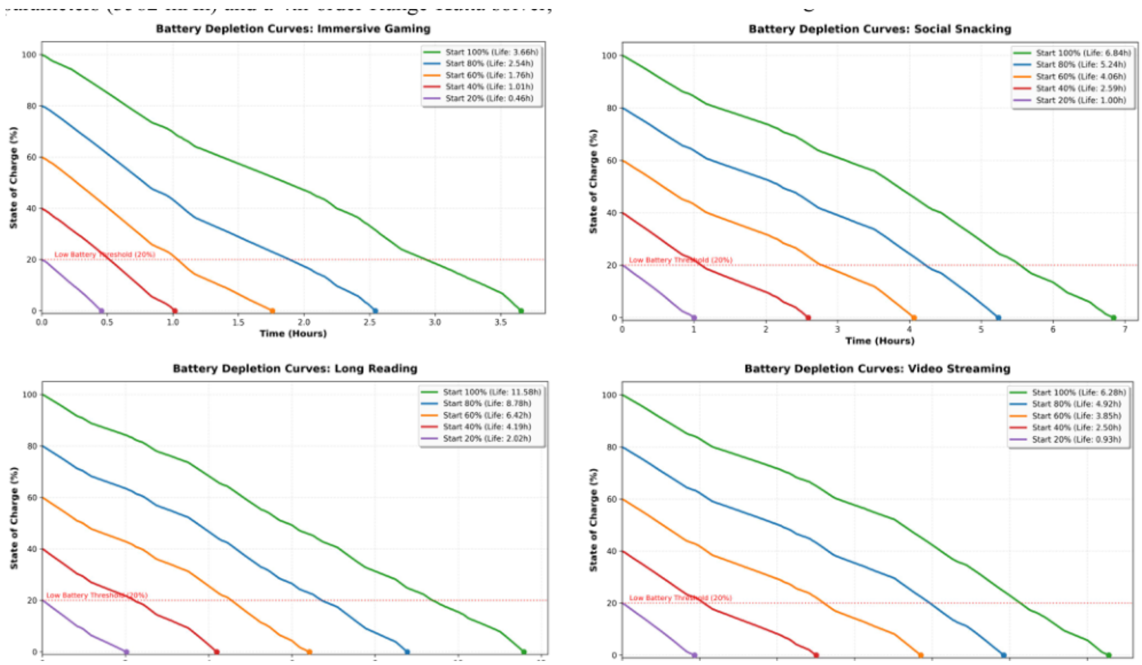

FIGURE 2. Battery depletion curves under four typical scenarios

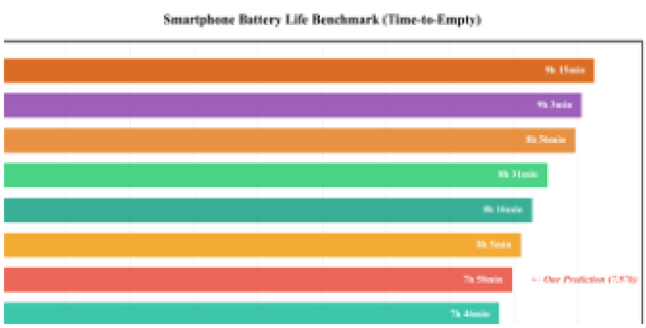

FIGURE 3. Smartphone battery life benchmark comparison

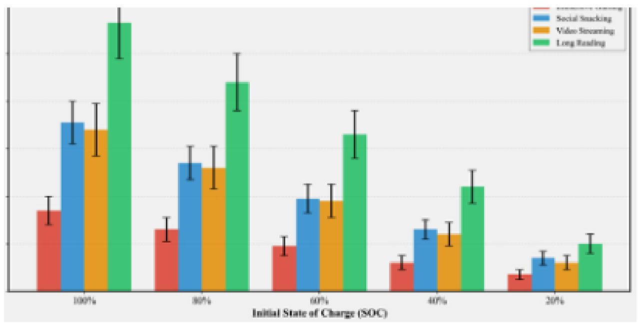

FIGURE 4. TTE distribution with 95% confidence intervals

lifetime, we introduce the concept of State of Health (SOH), defined as:

$$\mathrm{SOH} = \frac{Q_{\max}}{Q_{\text{design}}} \times 100\% = \left(1 - \frac{Q_{\text{loss}}}{Q_{\text{design}}}\right) \times 100\% \quad (27)$$

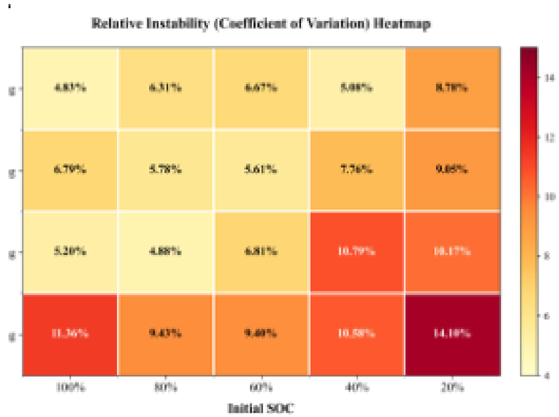

FIGURE 5. Relative instability (coefficient of variation) heatmap

Where $Q_{\max}$ represents the measurable capacity, Q_{design} is the nominal capacity at beginning-of-life, and the Q_{loss} is the capacity loss.To capture the nonlinear degradation dynamics under varying operating conditions, we adopt the cycle-based Wang model [21], which explicitly accounts for the coupled effects of cycle number N, discharge rate (C-rate), and temperature T and temperature. The capacity loss expression is reformulated as:

$$Q_{\text{loss}}(N, T, C\text{-rate}) = B \cdot \exp\left[-\frac{E_a(C\text{-rate})}{R \cdot T}\right] \cdot N^{0.552} \quad (28)$$

Where B is the pre-exponential degradation coefficient, $E_a(C\text{-rate})$ is the C-rate-dependent activation energy, R is the universal gas constant, and the exponent 0.552 reflects the decelerating degradation characteristic of SEI layer

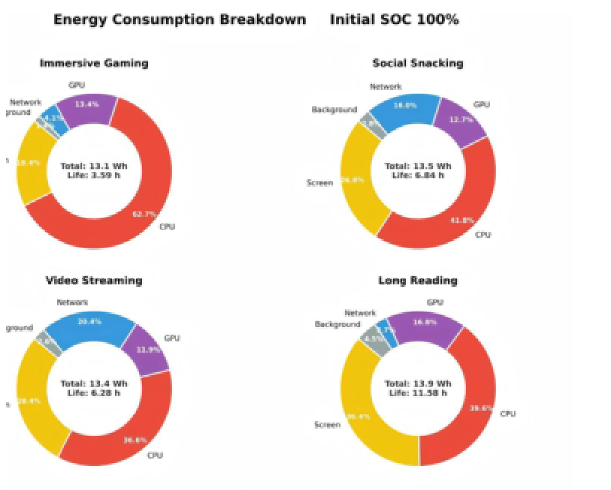

FIGURE 6. Energy consumption breakdown of four typical scenarios

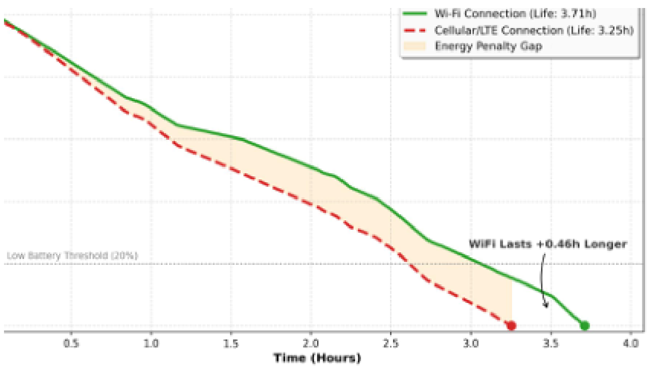

FIGURE 7. SOC decay trajectories under WiFi and cellular networks

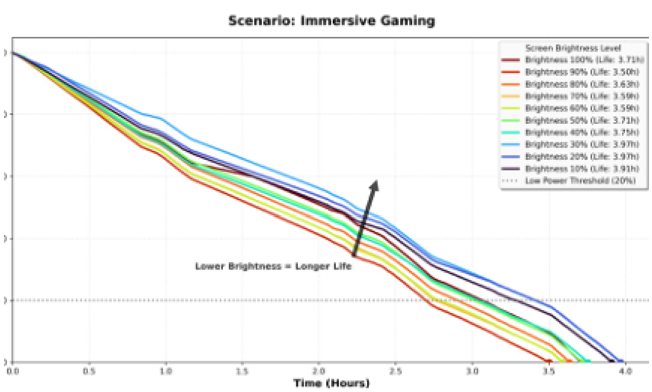

FIGURE 8. Screen Brightness (immersive gaming)

passivation. We define a normalized aging factor δ that quantifies the fractional retention of usable capacity:

$$\delta(N, T, C\text{-rate}) = 1 - \frac{Q_{\text{loss}}(N, T, C\text{-rate})}{Q_{\text{design}}} \tag{29}$$

This aging factor, which is numerically equal to SOH, directly modulates the effective capacity in the SOC dynamics. After accounting for cycle-dependent capacity fade, the modified SOC state update equation becomes:

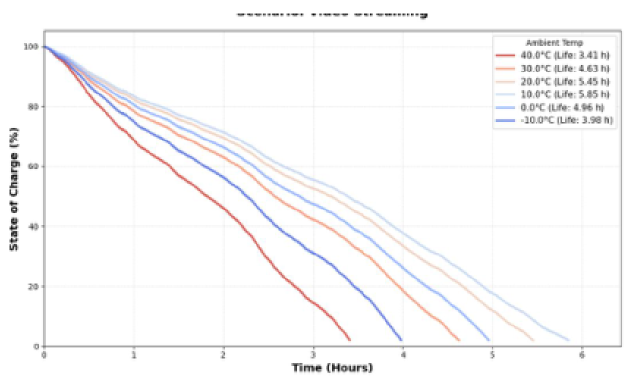

FIGURE 9. Seasonal impact on battery life (video streaming scenario)

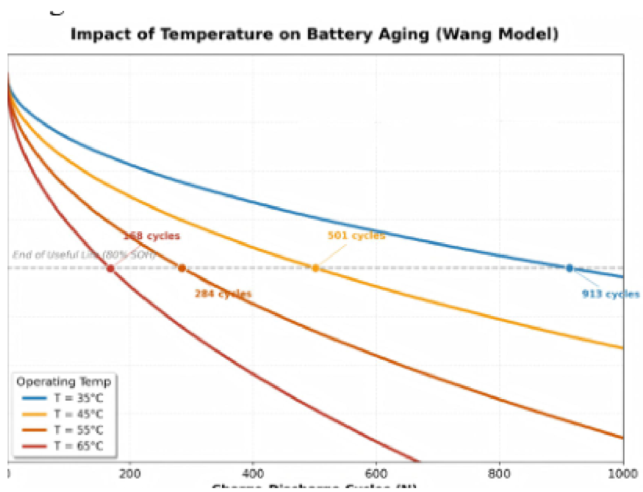

FIGURE 10. Impact of temperature on battery aging (Wang Model)

$$\frac{d\text{SOC}}{dt} = -\frac{I(t)}{\delta(N, T, C\text{-rate}) \cdot Q_{\text{nominal}}} \tag{30}$$

Where $I(t) > 0$ during discharge, and the denominator $\delta(N, T, C\text{-rate}) \cdot Q_{\text{nominal}}$ represents the age-adjusted effective capacity. This coupled electrothermal-aging framework enables long-term predictive modeling of battery life under realistic smartphone usage scenarios, with the model's dependency on observable quantities $(N, T, C\text{-rate})$ making it directly implementable in battery management systems.

B. IMPACT OF TEMPERATURE ON CYCLE LIFE

We further simulated the impact of different operating temperatures on the battery's full life cycle. The results are shown in Figure 10.

The results demonstrate the importance of thermal management for extending battery life. If the battery operates at 65°C for extended periods, the SOH falls below the industrial scrap standard of 80% after only 168 cycles. In contrast, if the operating temperature is controlled at

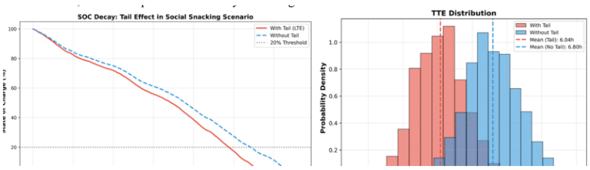

FIGURE 11. TTE distribution with and without wake effect

35°C, the battery life extends to 913 cycles, a 5.4-fold improvement.

V. SENSITIVITY ANALYSIS

This section evaluates the robustness of the proposed model under various perturbations and identifies the key factors driving battery depletion. Although the continuous-time differential-equation-based power model captures the dynamic behavior of battery discharge, its predictive accuracy is limited by modeling assumptions, parameter uncertainty, and the stochastic nature of user behavior. Therefore, a systematic sensitivity analysis is conducted from three perspectives: modeling assumptions, parameter perturbations, and usage pattern variability.

A. SENSITIVITY TO THE COMMUNICATION TAIL ASSUMPTION

In this model, while keeping all other parameters and usage patterns identical, we compare the battery discharge processes under two different settings: one that explicitly accounts for the "Tail Effect" of communication and one that neglects it. Further Monte Carlo simulations show that compared with the model without the "Tail Effect", the average Time to Exhaustion (TTE) is significantly reduced when the "Tail Effect" is considered. The results are shown in Figure 11.

B. SENSITIVITY TO POWER PARAMETER VARIATIONS

To assess the model's response to parameter uncertainty under high-load scenarios such as immersive gaming, proportional perturbations of $\pm 20\%$ are applied to three key power components: processor power, display power, and network power. The resulting changes in TTE are then evaluated. The tornado diagram of parameter sensitivity is shown in Figure 12.

C. SENSITIVITY TO USAGE PATTERN VOLATILITY

With model parameters held constant, three levels of usage volatility are considered: low volatility ($\sigma = 0.1$), moderate volatility ($\sigma = 0.3$), and high volatility ($\sigma = 0.5$). Multiple random simulations are conducted for each case. The results are shown in Figure 13.

The results demonstrate that as σ increases, the mean TTE remains relatively stable, whereas the standard deviation and the width of the confidence interval increase significantly.

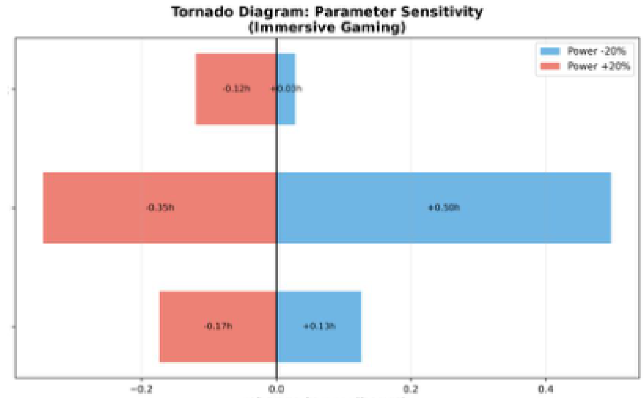

FIGURE 12. Tornado diagram of parameter sensitivity (immersive gaming)

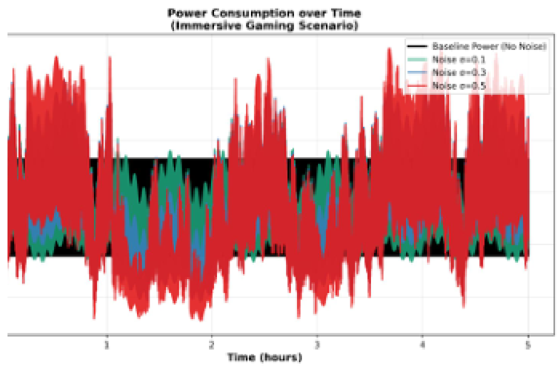

FIGURE 13. TTE distribution under different noise levels

D. DISCUSSION ON ASSUMPTION VALIDITY AND MODEL ROBUSTNESS

Overall, the proposed model demonstrates strong robustness and interpretability under multidimensional evaluation:

Structural robustness: The inclusion of the communication tail mechanism aligns the model more closely with the physical characteristics of mobile communication protocols.

Hierarchical responsiveness: The dominant factors identified through parameter sensitivity analysis are highly consistent with existing power decomposition studies.

Statistical reliability: The model naturally translates individual behavioral variability into probabilistic battery life predictions.

VI. CONCLUSIONS

This study systematically elucidates the intrinsic mechanisms of smartphone battery depletion by constructing an integrated model that combines nonlinear electrochemistry, thermodynamics, and stochastic load. The research not only achieves precise predictions of battery life across multiple scenarios but also quantitatively reveals the contribution rates of temperature, network traces, and stochastic behavior to energy loss. Based on these findings, energy optimization schemes are proposed at both the user and system levels.

Limitations and Future Research Directions: Although the model demonstrates good robustness, the current parameter calibration is still based on a specific hardware platform, and there is a lack of coverage for micro-level energy consumption differences between devices of different brands. Additionally, the model simplifies the complex resource scheduling logic under multi-task coordination to a significant extent. Future research will attempt to integrate more sensor data to correct stochastic process parameters in real time, and explore the transfer of this electro-thermal coupling framework to other lithium-battery-powered portable devices, such as tablets and drones, to achieve universal energy management across platforms.

DECLARATION OF CONFLICTING INTERESTS

The author(s) declared no potential conflicts of interest with respect to the research, author-ship, and/or publication of this article.

DATA SHARING AGREEMENT

The datasets used and/or analyzed during the current study are available from the corresponding author on reasonable request.

FUNDING

The author(s) received no financial support for the research, authorship, and/or publication of this article.

REFERENCES

[1] K. Huang, X. Zhang, Y. Guo, et al., "Source domain selection with early-cycle features for transfer learning-based prediction of lithium-ion battery degradation trajectories," Energy, vol. 344, Art. no. 139928, 2026, doi: https://doi.org/10.1016/J.ENERGY.2026.139928.

[2] A. P. Kharade, B. R. Mohite, J. Janardhanan, et al., "Improving the charging system and battery health of electric vehicles using AC-DC power factor correction resonant converters," Electrical Engineering, vol. 108, no. 2, Art. no. 121, 2026, doi: https://doi.org/10.1007/S00202-025-03506-9.

[3] S. A. Mijailovic, C. Gan, and W. B. Sheldon, "Scaling Models for Coupled Intercalation Dynamics, Electrolyte Depletion, and Lithium Plating during Fast Charging," Journal of The Electrochemical Society, vol. 173, no. 1, Art. no. 010507, 2026, doi: https://doi.org/10.1149/1945-7111/AE2A73.

[4] G. Shin and J. Kang, "Data-Driven Machine Learning Model for Battery Life Prediction Across Electrode Materials," International Journal of Energy Research, vol. 2026, no. 1, Art. no. 8083561, 2026, doi: https://doi.org/10.1155/ER/8083561.

[5] Y. Xie, J. Ding, W. Li, et al., "An improved thermal control strategy for raising energy efficiency and battery life in electric vehicles," Energy, vol. 344, Art. no. 139806, 2026, doi: https://doi.org/10.1016/J.ENERGY.2025.139806.

[6] A. Aranizadeh, B. Vahidi, and A. Khorsandi, "Extending battery health in wind-integrated systems through optimal state of charge management: A multi-objective approach," Journal of Energy Storage, vol. 146, Art. no. 119980, 2026, doi: https://doi.org/10.1016/J.EST.2025.119980.

[7] X. Li, H. Zhang, C. Liu, et al., "Hierarchical real-time energy management strategy of eVTOL hybrid power system based on finite-set," Aerospace Science and Technology, vol. 170, Art. no. 111546, 2026, doi: https://doi.org/10.1016/J.AST.2025.111546.

[8] B. Kavasogullari and E. M. Karagoz, "Numerical study on the heat transfer enhancement and fin size optimization of hybrid battery thermal management system," Physica Scripta, vol. 101, no. 1, Art. no. 015209, 2026, doi: https://doi.org/10.1088/1402-4896/AE2DDC.

[9] S. E. Park, X. Liu, J. H. Hwang, et al., "Deep Convolutional Neural Network-Based Detection of Gait Abnormalities in Parkinson's Disease Using Fewer Plantar Sensors in a Smart Insole," Biosensors, vol. 16, no. 1, Art. no. 40, 2026, doi: https://doi.org/10.3390/BIOS16010040.

[10] W. Zhou, B. Li, and X. Zeng, "Intrusion detection model of UAV system based on machine learning and neural network," Frontiers in Physics, vol. 13, Art. no. 1660104, 2026, doi: https://doi.org/10.3389/FPHY.2025.1660104.

[11] A. J. Lee, J. H. Kim, and M. K. Oh, "Exploring Wearable Device Use Among Dementia Caregivers: Benefits, Challenges, and Improvements," Innovation in Aging, vol. 9, no. Supplement_2, 2025, doi: https://doi.org/10.1093/GERONI/IGAF122.3466.

[12] L. Zhang, Z. Zhang, C. Hou, et al., "Lossless Information-Based Dimensionality Reduction of Comprehensive Features With a Deep Variational Autoencoder Enables Early-Life Prediction of Lithium-Ion Batteries," Carbon Neutralization, vol. 5, no. 1, Art. no. e70097, 2025, doi: https://doi.org/10.1002/CNL2.70097.

[13] Z. Ding, Q. Xiang, C. Li, et al., "Dynamic Boundary Optimization via IDBO-VMD: A Novel Power Allocation Strategy for Hybrid Energy Storage with Enhanced Grid Stability," Energy Engineering, vol. 123, no. 1, 2025, doi: https://doi.org/10.32604/EE.2025.070442.

[14] G. Chen, H. Zhou, J. Yang, et al., "Optimization of open-circuit voltage curve acquisition and state estimation for aging lithium-ion batteries," Energy, vol. 342, Art. no. 139606, 2026, doi: https://doi.org/10.1016/J.ENERGY.2025.139606.

[15] H. Liu, H. Jing, Y. Chen, et al., "Integrating vertical magnetic fields for safe lithium metal batteries with fast lithium-ion kinetics," Journal of Power Sources, vol. 666, Art. no. 239080, 2026, doi: https://doi.org/10.1016/J.JPOWSOUR.2025.239080.

[16] N. Xie, W. Zhao, Z. Wang, et al., "An eco-friendly dual-layer parallel control strategy for intelligent hybrid truck platoon considering sustainable emission management and energy optimization," Process Safety and Environmental Protection, vol. 206, Art. no. 108321, 2026, doi: https://doi.org/10.1016/J.PSEP.2025.108321.

[17] R. S. Ghatak, S. Tripathy, N. C. Bhende, et al., "Collaborative planning and scheduling framework of EV charging infrastructure with Vehicle-to-Grid facility in a renewable integrated smart grid," Computers and Electrical Engineering, vol. 130, Art. no. 110911, 2026, doi: https://doi.org/10.1016/J.COMPELECENG.2025.110911.

[18] M. M. S. Gazafrudi, Y. Darvishpour, and S. Farsi, "Hybrid ANFIS-BiLSTM-ANFIS model for remaining useful life prediction of Li-ion batteries in electric trains," Results in Engineering, vol. 29, Art. no. 108690, 2026, doi: https://doi.org/10.1016/J.RINENG.2025.108690.

[19] Z. Cao, Z. Wu, and J. Gray, "RFID Tag-Integrated Multi-Sensors with AIoT Cloud Platform for Food Quality Analysis," Electronics, vol. 15, no. 1, Art. no. 106, 2025, doi: https://doi.org/10.3390/ELECTRONICS15010106.

[20] H. Cheng, S. Liu, X. Zhang, et al., "Research on the Development Status, Challenges, and Trends of Electric Ferries in China under the Background of Carbon Neutrality," Journal of Power and Energy Engineering, vol. 13, no. 12, pp. 80–102, 2025, doi: https://doi.org/10.4236/JPEE.2025.1312007.

[21] J. Wang, P. Liu, J. Hicks-Garner, E. Sherman, S. Soukiazian, M. Verbrugge, H. Tataria, J. Musser, and P. Finamore, "Cycle-life model for graphite-LiFePO4 cells," Journal of Power Sources, vol. 196, no. 8, pp. 3942–3948, 2011, doi: https://doi.org/10.1016/j.jpowsour.2010.11.134.